THE ASTROPHYSICAL JOURNAL, 494:759–767, 1998 February 20

TESTING THE WHITE DWARF MASS-RADIUS RELATION WITH *HIPPARCOS*[1]

J. L. PROVENCAL AND H. L. SHIPMAN
Department of Physics and Astronomy, University of Delaware, Newark, DE 19716; jlp@strauss.udel.edu
ERIK HØG
Copenhagen University Observatory, Juliane Maries Vej 30, DK 2100 Copenhagen Ø, Denmark
AND
P. THEJLL
Nordita, Blegdamsvej 17, Copenhagen Ø, Denmark; present address, Danish Meteorological Institute, Lyngbyvej 100, DK-2100 Copenhagen Ø, Denmark
Received 1997 July 3; accepted 1997 September 30

ABSTRACT

We present the *Hipparcos* parallaxes and resulting radii for 10 white dwarfs in visual binaries or common proper-motion systems and 11 field white dwarfs. For bright stars, *Hipparcos* parallaxes have uncertainties approaching 1 mas and are thus considerably more accurate than earlier ground-based parallaxes. Overall, our results support the predictions of the white dwarf mass-radius relation and our understanding of stellar degeneracy. Our most important finding for an individual object is the position of 40 Eri B, a well-known puzzle, now consistent with single-star evolution. In addition, we present evidence supporting the existence of a range of atmosphere thicknesses for hydrogen (DA) white dwarfs.

Subject headings: astrometry — stars: fundamental parameters — stars: individual (40 Eridani B) — ultraviolet: stars — white dwarfs

1. INTRODUCTION

The *Hipparcos* Space Astrometry mission (European Space Agency 1997) is dedicated to the precise measurement of the positions, parallaxes, and proper motions of nearly 120,000 stars. Over 1000 Gbytes of data were returned during the spacecraft's 3 yr lifetime, making the production of the catalogs one of the largest analysis endeavors ever undertaken. *Hipparcos* parallaxes, with accuracies approaching 1 mas for brighter stars, will have significant impact on a broad range of astrophysical fields. We focus here on approximately 20 white dwarfs, either single or members of binary systems, included in the *Hipparcos* input catalog (European Space Agency 1997). In particular, we will use *Hipparcos* parallaxes to test the white dwarf mass-radius relation directly.

Chandrasekhar first published his Nobel Prize–winning description of the equation of state for electron degenerate material comprising white dwarfs in 1933, predicting the existence of a relationship between mass and radius for a degenerate configuration. This theoretical mass-radius relation, incorporating the improvements of Hamada & Salpeter (1961) and Wood (1990, 1995), is a generally accepted underlying assumption in nearly all studies of white dwarf properties. In turn, these studies, including, for example, the white dwarf mass distribution and luminosity function, are foundations for such varied fields as stellar evolution and galactic formation.

One might assume that a theory as basic as stellar degeneracy rests on solid observational grounds, yet this is not the case. Comparison between observation and theory has shown disturbing discrepancies (Schmidt 1996; Provencal et al. 1997). Critical problems with the observational results include independent determinations of masses, especially for single white dwarfs, and accurate distances from which precise stellar radii can be derived. In addition, white dwarfs span a relatively narrow mass distribution centered on approximately 0.6 $M_{\odot}$ (Bergeron, Saffer, & Liebert 1992, hereafter BSL). Few objects are available for testing the mass-radius relation at either the high- or low-mass extremes.

The most general method used to determine white dwarf masses, and the single technique capable of inferring the masses of solitary white dwarfs, is the comparison of observed spectra with the predictions of model atmospheres. This comparison produces estimates of surface gravity (log g) and effective temperatures by matching the widths of line profiles. Precise surface gravities are essential, as the uncertainty in log g translates directly into the mass uncertainty (Schmidt 1996). However, surface gravity is a function both of mass and of radius. Most field white dwarfs do not have the accurate parallax measurements necessary for deriving precise independent radii. In most cases, to determine stellar mass one must assume an underlying mass-radius relation for a given core composition, usually chosen to be carbon. It is therefore difficult to prove the validity of the mass-radius relation without pre-assuming its existence. An additional piece of information is needed.

The best direct test of stellar degeneracy is the determination of radii for white dwarfs in visual binaries (Table 1). In these cases, white dwarf masses are well determined from their orbital parameters, and stellar radii are derived from knowledge of effective temperatures and distances. Since knowledge of the stellar mass represents the additional information we lack for single stars, it is not necessary to assume a mass-radius relation, making these systems excellent tests of stellar degeneracy. However, visual binaries with well-determined orbital parameters and accurate parallax measurements are relatively rare. Observational support of stellar degeneracy rests on the four objects in Table 1 for which ground- or space-based measurements are sufficient for determining the white dwarf's characteristics: 40 Eri B (Koester & Weidemann 1991), Stein 2051 B (Strand 1977; Liebert 1976), Sirius B (Shipman 1979), and

[1] Based on data from the ESA *Hipparcos* astrometry satellite.

TABLE 1

WHITE DWARFS IN WIDE BINARY SYSTEMS PRE-*Hipparcos*

Object	π (mas)	Mass ($M_\odot$)	Radius ($R_\odot$)	P_{orbit} (yr)
Sirius B	375.6 ± 3.0 (G)	1.03 ± 0.015	0.0074 ± 0.0007	50.09
	379.2 ± 1.6 (H)	...	...	...
Stein 2051B.....	181.2 ± 1.1 (G)	0.48 ± 0.045	0.0111 ± 0.0015	>300
	181.4 ± 3.7(H)	...	...	...
40 Eri B.....	208.4 ± 2.3 (G)	0.43 ± 0.02 (astro)	0.0124 ± 0.0005	>300
	198.24 ± 0.84 (H)	0.53 ± 0.04 (spec)	0.0127 ± 0.002	...
G107-70AB	88.3 ± 2.5 (G)	0.65 ± 0.15	...	20.5 ± 1.9
	88.3 ± 2.5 (H)	0.64 ± 0.15	...	...
Procyon B	286.4 ± 2.3 (G)	0.594 ± 0.012	0.0096 ± 0.0005	40.5
	285.9 ± 0.9 (H)	...	...	...

NOTES.—The labels "G" and "H" refer to ground-based and *Hipparcos* parallaxes, respectively. The ground-based parallaxes are those used in previous studies of the mass-radius relation, and do not necessarily represent the best ground-based measurements available. Both the spectroscopic and astrometric masses for 40 Eri B are given.

REFERENCES.—Girard et al. 1996; Harrington et al. 1993; Shipman 1979; Shipman & Sass 1980; Koester & Weidemann 1991; Liebert 1976; Bois, Mochnacki, & Lanning 1988; Borgman & Lippincott 1983; and Heintz 1974.

Procyon B (Provencal et al. 1997). The ground-based parallaxes quoted in Table 1 and used in Figure 1 are those used in the above-mentioned references for previous studies of the mass-radius relation. They do not necessarily represent the best ground-based parallaxes available today. Figure 1 presents the disturbing state of affairs prior to *Hipparcos*. There are too few points (only four), and three of the four stars fall 1.5 σ below the expected relation.

General relativity introduced gravitational redshift velocity measurements as a second method of determining white dwarf masses without necessarily invoking the mass-radius relation (Wegner & Reid 1987). Currently, gravitational redshift measurements are confined by our limited understanding of atomic physics to hydrogen atmosphere (DA) white dwarfs. The non-LTE core of Hα is commonly used, as the other hydrogen lines are more strongly affected by pressure shifts (Grabowski, Madej, & Halenka 1987). Since this technique requires precise knowledge of the white dwarf's physical velocity to distinguish gravitational velocity shifts from the Doppler effect, a common approach is to use white dwarfs in wide binaries or common proper-motion (CPM) pairs in which the system velocity can be accurately determined from the companion. As with surface gravity, gravitational radial velocity is a function both of mass and of radius, requiring either an independent radius determination or an assumed relationship between mass and radius. Stellar radii of nearby stars can be derived using effective temperatures and distances.

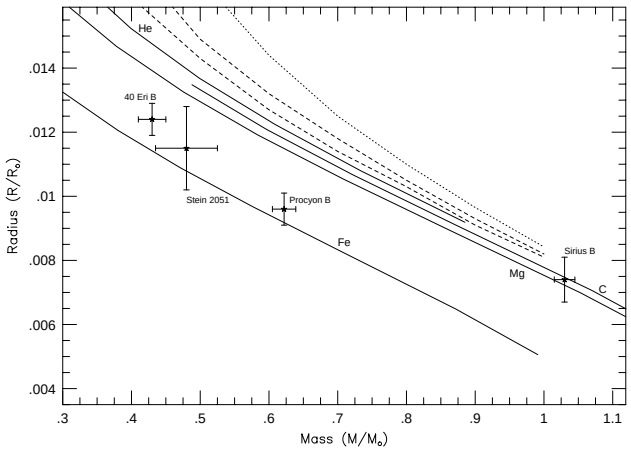

FIG. 1.—Observational support for the white dwarf mass-radius relation prior to *Hipparcos*. The solid lines labeled He, C, Mg, and Fe denote the zero-temperature mass-radius relation of Hamada & Salpeter. The dotted line is a 30,000 K hydrogen atmosphere Wood (1995) relation, and the dashed lines are Wood (1995) relations for 15,000 and 8000 K hydrogen-surface white dwarfs. The 1 σ error bars mark the observed points.

Underlying the above discussion is the importance of accurate distance measurements for determining white dwarf masses and radii. Yet, parallax remains simultaneously one of the most important and most uncertain physical parameters. It is the dominant source of the error bars displayed in Figure 1. In 1982, one of the authors (H. L. S.) proposed a number of targets for the *Hipparcos* mission in order to help address the above considerations, first by improving the observed parallaxes for the visual binaries, and second, by increasing the observed sample by obtaining accurate parallaxes for white dwarfs with gravitational redshift mass determinations. In this paper we present the results of these observations. We outline the results for visual binaries, CPM pairs, and field white dwarfs, and discuss the implications for the white dwarf mass-radius relation.

2. THE DATA

Hipparcos is a unique astronomical observatory. The primary instrument is a 29 cm all-reflective Schmidt telescope. A split mirror combines two fields of view, separated by approximately 58°, into a single focal grid. The satellite spins once every 128 minutes, allowing target stars to traverse the grid. The resulting light modulation is recorded by a photon-counting image dissector tube. The sampling rate is 1/1200 s^{-1}, and each measurement contains between 128 and 2650 individual measurements (Perryman et al. 1992). This interesting configuration allows for the measurement of one-dimensional relative positions of target stars with respect to other stars in the scan direction.

The extensive reduction techniques transforming photon counts to astrometric and photometric results are discussed in detail in Lindegren et al. (1992). In brief, the reductions involve an iterative process, reassembling positional and photometric information into a system of positions, dis-

tances, and space motions. All reductions are performed by the *Hipparcos* data analysis consortiums (Lindegren et al. 1992; Kovalevsky et al. 1992). The original proposer receives a list containing *Hipparcos* identification numbers, positions, photometric information, and parallaxes with associated errors. The errors are standard products of the *Hipparcos* data-reduction procedure, robustly determined and dependent on the square root of available observing time.

3. THE WHITE DWARF MASS-RADIUS RELATION

3.1. *Visual Binaries*

The *Hipparcos* input catalog includes the important visual binaries Sirius, Procyon, 40 Eri, and Stein 2051. We concentrate here on Sirius, Procyon, and 40 Eri B. Stein 2051's *Hipparcos* parallax agrees with—but is less accurate than—its ground-based determination.

Sirius, Procyon, 40 Eri, and Stein 2051 represent the shaky underpinnings of the empirical white dwarf mass-radius relation. It is important that we understand why three of the four points do not lie near the expected relation. Our goals therefore include understanding the various contributions to the total error budget for each object, the reduction of error bars, and verification of ground-based parallaxes, especially for 40 Eri B. The discrepancy between astrometric and spectroscopic mass determinations for this mysterious white dwarf is discussed extensively in the literature (Shipman et al. 1997 and references therein). In Table 1 we present the relevant white dwarf physical parameters, including the *Hipparcos* parallaxes, which are a factor of 2 more accurate than previous determinations.

For the most part, the *Hipparcos* parallaxes agree with the ground-based estimates to within 1 σ. A more detailed general discussion of ground-based versus *Hipparcos* parallaxes can be found in Vauclair et al. (1997). Comparing our corresponding values in Table 1, we find a 1% increase for Sirius, essentially no change for Stein 2051, a 0.2% decrease for Procyon, and a 5% decrease for 40 Eri. The new values, taken in tandem with the reduced error estimates, are significant when reconsidering the white dwarf masses and radii.

Calculations of mass employ Kepler's third law. The most direct method of determining radii, discussed in detail in Shipman (1979), is

$$f_\lambda = 4\pi H_\lambda R^2/D^2 \ . \tag{1}$$

These two calculations utilize six parameters: the apparent semimajor axis a, the orbital period P, the parallax π, the fractional mass f, the monochromatic stellar flux H_λ, and the stellar flux f_λ. Tables 1 and 2 present the best observed values for Procyon B, Sirius B, and 40 Eri B. Redetermining masses and radii merely involves placing the correct observed quantities in the appropriate equation and solving either for M or for R.

Let us first consider mass, which depends strongly on parallax ($M \propto \pi^{-3}$). As the distance increases, the actual separation follows, leading to a corresponding increase in stellar mass. The *Hipparcos* parallaxes translate into a mass decrease of 3% for Sirius B, an increase of 0.5% for Procyon B, and a large 14% increase for 40 Eri B.

The relationship between radius, stellar flux, monochromatic flux, and distance is given by equation (1). Stellar flux is generally determined from visual magnitude. Its corresponding error is a combination of random and systematic errors resulting from the transformation of magnitude (m_v) to flux. Shipman (1979) argues that, regardless of the accuracy of m_v within its own internal system, there remains a residual 2% uncertainty, resulting from the conversion of m_v to absolute flux. H_λ is a function of effective temperature and is taken from Bergeron, Wesemael, & Beauchamp (1995b).

As our goals include understanding the contributions of the different parameters to each visual binary's overall error budget, we consider it important to track the sources of error through our calculations. Each parameter's contribution is best understood by applying standard error propagation techniques to the above relations, assuming statistical independence of all sources of uncertainty:

$$\frac{\Delta M}{M} = \left[\left(3\frac{\Delta a}{a}\right)^2 + \left(2\frac{\Delta P}{P}\right)^2 + \left(3\frac{\Delta \pi}{\pi}\right)^2 + \left(\frac{\Delta f}{f}\right)^2\right]^{1/2}, \tag{2}$$

$$\frac{\Delta R}{R} = \left[\left(\frac{1}{2}\frac{\Delta f_\lambda}{f_\lambda}\right)^2 + \left(\frac{1}{2}\frac{\Delta H_\lambda}{H_\lambda}\right)^2 + \left(\frac{\Delta \pi}{\pi}\right)^2\right]^{1/2} . \tag{3}$$

We present the revised masses, radii, and error contributions for Sirius B, Procyon B, and 40 Eri B in Table 3. The change in Sirius B's radius from published values of 0.0074 ± 0.0007 $R_\odot$ (Provencal et al. 1997) to 0.0084 ± 0.0002 $R_\odot$ results largely from our use of the improved temperature of $24{,}700 \pm 300$ K (Kidder 1991). Previous radius determinations (Shipman 1979) used the higher temperature of $29{,}000 \pm 1000$ K. The change in 40 Eri B's astrometric mass from 0.43 ± 0.02 $M_\odot$ to 0.501 ± 0.011 $M_\odot$ results from the change in parallax (Shipman et al. 1997). As we hoped, the masses and radii for all three visual binaries show improved overall accuracy. While parallax remains a significant source of mass error, the importance of the additional parameters for individual stars is clear. Uncertainty in separation is the major contributor to Procyon B's mass uncertainty. In contrast, 40 Eri B's mass estimate could be improved by a better flux (magnitude) determination.

Table 3 clearly demonstrates that parallax now contributes only a small portion of the radius error budget. The

TABLE 2

VISUAL BINARIES OBSERVED PARAMETERS

Object	m_v	$T_{\rm eff}$ (K)	Separation (arcsec)	Fractional Mass
Sirius B	8.44 ± 0.05	24700 ± 300	7.56 ± 0.01	0.3295 ± 0.0010
40 Eri B	9.50 ± 0.02	16700 ± 300	6943 ± 6.4	0.738 ± 0.01
Procyon B.....	10.92 ± 0.05	8688 ± 200	4.271 ± 0.041	0.288 ± 0.001

REFERENCES.—Shipman et al. 1997; Gatewood & Gatewood 1978; Girard et al. 1996; and Provencal et al. (1997).

TABLE 3

VISUAL BINARIES: REVISED MASSES, RADII, AND ERROR CONTRIBUTIONS

Parameter	Procyon B	Sirius B	40 Eri B
Mass ($M_\odot$)	0.604 ± 0.018	1.000 ± 0.016	0.501 ± 0.011
Error Budget			
$3(\Delta a/a)$	0.0288	0.008	0.0028
$2(\Delta P/P)$	0.0029	0.002	0.0022
$3(\Delta\pi/\pi)$	0.009	0.0126	0.015
$\Delta f/f$	0.003	0.003	0.013
Net Error $\Delta M/M$	0.0305	0.0154	0.022
Radius ($R_\odot$)	0.0096 ± 0.0004	0.0084 ± 0.0002	0.0136 ± 0.0002
Error Budget			
$\Delta f_\lambda/2f_\lambda$	0.0235	0.0235	0.01
$\Delta H_\lambda/2H_\lambda$[a]	0.0336	0.0107	0.009
$\Delta\pi/\pi$	0.0031	0.0042	0.005
Net Error $\Delta R/R$	0.0411	0.026	0.017

NOTE.—Error budget values are for Eqs. 2 and 3.

REFERENCES.—Shipman et al. 1997 (40 Eri B); Girard et al. 1996 (Procyon B); and Gatewood & Gatewood 1978 (Sirius B).

[a] H_λ includes T.

dominant radius error contributors are flux and effective temperature (through H_λ).

3.2. *Common Proper-Motion Pairs with Gravitational Redshift Masses*

As we discussed in the introduction, general relativity provides a second, verifiable method of determining mass. Gravitational redshift velocity is a function both of mass and of radius, requiring either an independent radius determination or a second relationship between mass and radius:

$$v_g = 0.635(M/M_\odot)(R_\odot/R) \text{ km s}^{-1} . \quad (4)$$

Prior to *Hipparcos*, very few CPM systems used in gravitational redshift velocity studies had accurate trigonometric parallaxes leading to a radius determination via effective temperatures and distances. In the majority of cases, the only approach was to invoke a mass-radius relation, rendering the measurements unsuitable for testing the white dwarf mass-radius relation directly.

The *Hipparcos* input catalog includes seven CPM pairs (Table 4) in which the white dwarf has a gravitational redshift velocity determination (Reid 1996). We combine the parallaxes, temperatures, and published redshift velocities of these objects to determine radii following equation (1). We then use these radii to solve equation (4) for mass.

Table 5 presents the current gravitational masses, radii, and error budgets for the seven CPM systems. The quoted mass errors are produced by the application of standard error propagation techniques to equation (4), and in most cases they are more generous than previously published estimates. Radius errors result from the procedures outlined in § 3.1. The CPM systems are both more distant and fainter than the visual binaries. Therefore their *Hipparcos* paral-

TABLE 4

CPM WHITE DWARFS OBSERVED PARAMETERS

Object	$T_{\rm eff}$ (1000 K)	m_v	π (mas)	v_g (km s^{-1})
CD−38 10980.....	24.0 ± 0.2	10.98 ± 0.03	78.0 ± 2.4	37.9 ± 2.0
Wolf 485A	14.1 ± 0.4	12.31 ± 0.03	55.5 ± 3.8	24.9 ± 3.2
L268-92	11.8 ± 1.0	13.47 ± 0.05	38.0 ± 0.8	30.2 ± 5.0
G154-B5B.....	14.0 ± 0.4	14.22 ± 0.07	26.9 ± 3.8	22.6 ± 2.1
G181-B5B.....	13.6 ± 0.5	15.9 ± 0.1	14.6 ± 1.0	29.0 ± 0.8
G156-64	7.16 ± 0.2	16.50 ± 0.05	$28.7 \pm 1.3°$	34.1 ± 2.5
L481-60	11.3 ± 0.3	12.85 ± 0.05	65.6 ± 0.8	27.9 ± 3.2

NOTE.—m_v is the visual magnitude, and v_g is the gravitational redshift velocity.

REFERENCES.—Koester 1987; Wegner & Reid 1991; Reid 1996; and BSL.

TABLE 5

CPM WHITE DWARF MASSES, RADII, AND ERROR CONTRIBUTIONS

Parameter	CD−38 10980	W485A	L268-92	L481-60	G154-B5B	G181-B5B	G156-64
Mass ($M_\odot$)	0.74 ± 0.04	0.59 ± 0.04	0.70 ± 0.12	0.53 ± 0.05	0.46 ± 0.08	0.50 ± 0.05	0.59 ± 0.06
Radius ($R_\odot$)	0.01245 ± 0.0004	0.0150 ± 0.001	0.0149 ± 0.001	0.1200 ± 0.0004	0.130 ± 0.002	0.011 ± 0.001	0.0110 ± 0.001
Error Budget							
$\Delta f_\lambda/2f_\lambda$	0.009	0.024	0.024	0.024	0.033	0.048	0.048
$\Delta H_\lambda/2H_\lambda$[a]	0.008	0.013	0.069	0.020	0.022	0.030	0.054
$\Delta\pi/\pi$	0.031	0.068	0.021	0.0117	0.143	0.065	0.045
Net Radius Error.....	0.033	0.073	0.076	0.050	0.147	0.086	0.085

REFERENCES.—Landolt 1992; Holberg, Bruhweiler, & Andersen 1995; Reid 1996; BSL; and Kidder et al. 1991.

[a] H_λ includes T.

laxes are correspondingly smaller and less accurate, and remain a significant source of radius error. Table 5 also shows that significant radius error reductions could be achieved through improved temperatures and fluxes. CD −38 10980 represents the best-determined CPM object in our sample.

3.3. *The Radii of Field White Dwarfs*

The masses of field white dwarfs are commonly determined through spectroscopic analysis. A comparison of observed spectra with predictions of model atmospheres yields an estimate of stellar surface gravities (log g) and effective temperatures. However, like gravitational redshift velocity, log g depends both on mass and on radius:

$$M = \frac{gR^2}{G} . \quad (5)$$

Since the overwhelming majority of field white dwarfs do not have precise ground-based parallaxes, it is difficult to obtain accurate masses without relying on a mass-radius relation. For this reason, most white dwarf masses and radii obtained from surface gravities are not valid tests of the mass-radius relation.

Physical uncertainties associated with this spectroscopic comparison include pressure effects, such as the presence of helium, which mimics increased surface gravity, ambiguities surrounding convective efficiency, limitations of the broadening theory, and the unavoidable inaccuracies of observed parameters.

BSL, followed by Bragaglia, Renzine, & Bergeron (1995), attempt to lessen the severity of these uncertainties by restricting their samples to DA stars with effective temperatures above 15,000 K. At these temperatures white dwarf atmospheres are completely radiative, thereby reducing uncertainties resulting from convection itself, as well as minimizing the possible effects of convective dredge-up of underlying helium. The authors fit detailed model atmospheres to full Balmer line profiles to obtain log g and effective temperatures. The authors then derive masses based on Wood (1990, 1995) evolutionary models assuming carbon cores surrounded by a helium layer of log He = −4.

The *Hipparcos* input catalog includes a number of field white dwarfs. We focus here on the *Hipparcos* sample included in the studies of BSL and Bragaglia et al. (1995), because the two studies use similar fitting techniques to obtain log g. We combine the parallaxes and effective temperatures, as outlined in § 3.1, to derive radii for these stars. Armed with these radii, we use log g to retrieve stellar masses without invoking a mass-radius relation. Table 6 presents the relevant physical parameters for our sample of field white dwarfs, including *Hipparcos* parallaxes, ground-based parallaxes when available, and resulting radii. The quoted radius errors result from the application of standard error propagation techniques to equation 5. With the exceptions of G238-44 and G226-29, the *Hipparcos* and ground-based parallaxes agree to within $\approx 1\ \sigma$. The *Hipparcos* parallaxes are on average 1.8 times more accurate than the ground-based measurements.

4. TESTING THE MASS-RADIUS RELATION

We begin our discussion of observational support for the white dwarf mass-radius relation with Figure 1, displaying the situation prior to *Hipparcos*. The four visual binaries are represented by 1 σ error bars in mass and radius. The solid lines represent the Hamada-Salpeter (1961) zero-temperature mass-radius relations for core compositions of He, C, Mg, and Fe. The dotted line is a Wood (1995) mass-radius relation for models with temperatures of 30,000 K, carbon cores, and thick hydrogen atmospheres [log q(H) = −4]. The dashed lines represent 8000 and 15,000 K, carbon-core, thick–hydrogen atmosphere models. The agreement is not pleasing. Procyon B, Stein 2051 B, and 40 Eri B lie approximately 1.5 σ below their expected relations.

TABLE 6

FIELD WHITE DWARFS OBSERVED PARAMETERS

Object	π (mas)	$T_{\rm eff}$ (1000 K)	log g	Radius ($R_\odot$)
GD279	63.0 ± 3.8 (H)	13.5 ± 0.2	7.83 ± 0.03	0.0129 ± 0.0008
	61.0 ± 7.0 (G)			
Feige 22	41.5 ± 5.0 (H)	19.1 ± 0.4	7.78 ± 0.04	0.01367 ± 0.002
	45.0 ± 5.0 (G)			
EG 21	98.5 ± 1.5 (H)	16.2 ± 0.3	8.06 ± 0.05	0.0115 ± 0.0004
EG 50	64.9 ± 3.4 (H)	21.0 ± 0.3	8.10 ± 0.05	0.0104 ± 0.0006
	59.7 ± 4.0 (G)			
GD 140	65.3 ± 3.6 (H)	21.7 ± 0.3	8.48 ± 0.05	0.0085 ± 0.0005
	70.4 ± 10.9 (G)			
G238-44	40.3 ± 2.9 (H)	20.2 ± 0.4	7.90 ± 0.05	0.0120 ± 0.001
	30.5 ± 5.9 (G)			
G226-29	91.1 ± 2.3 (H)	12.0 ± 0.2	8.29 ± 0.03	0.0104 ± 0.0003
	82.7 ± 5.0 (G)			
WD2007-303.....	65.1 ± 3.9 (H)	15.2 ± 0.7	7.86 ± 0.05	0.0128 ± 0.001
Wolf 1346	67.7 ± 2.3 (H)	20.0 ± 0.3	7.83 ± 0.05	0.01342 ± 0.0006
	69.4 ± 2.3 (G)			
G93-48	39.8 ± 4.5 (H)	18.3 ± 0.3	8.02 ± 0.05	0.0141 ± 0.002
	40.8 ± 2.5 (G)			
L711-10	47.4 ± 4.0 (H)	19.9 ± 0.4	7.93 ± 0.05	0.0132 ± 0.001
	42.4 ± 8.4 (G)			

NOTE.— The labels "H" and "G" refer to *Hipparcos* and ground-based (where available) parallaxes, respectively.

REFERENCES.—BSL; Reid 1996; Bragaglia et al. 1995; Bergeron, Liebert, & Fulbright 1995a; Kepler et al. 1995; and van Altena, Lee, & Hoffleit 1995.

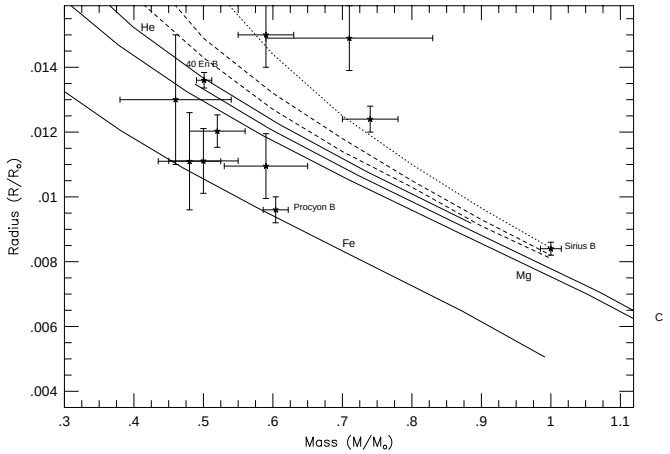

FIG. 2.—Observational support for the white dwarf mass-radius relation after *Hipparcos*, showing revised positions for the visual binaries and including results from the common proper-motion systems.

Figure 2 presents the revised visual binary positions, as well as the results for the CPM pairs. These objects test the mass-radius relation using the absolute minimum of physical assumptions. The physics underlying this figure is Kepler's third law, the gravitational redshift, and some general assumptions regarding the ability of model atmospheres to predict a value of the emergent flux H_λ. There are a considerably greater number of data points than presented in Figure 1, although many of the additions are somewhat uncertain. The important binaries, Sirius B, Procyon B, and 40 Eri B, are plotted with improved accuracy. Figure 3 repeats Figure 2, but also includes the field white dwarfs from Table 6. In addition to the physics underlying Figure 2, broadening theory must be included in the underlying assumptions for Figure 3.

Our first conclusion is that the mass-radius relation is now more firmly supported on observational grounds. For readers who like high-precision data points, Sirius B and 40 Eri B fit the theoretical relation quite precisely. For readers who enjoy an abundance of data points, Figure 3 more than quadruples the number of observed points, the majority of which lie between 1 and 2 σ from the Wood models. We discuss the discrepant points below.

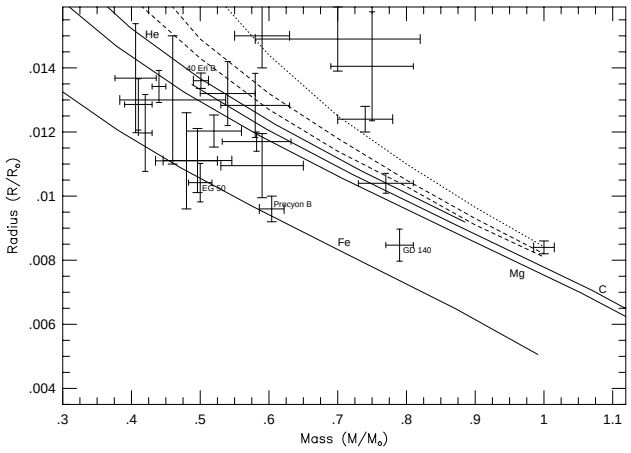

FIG. 3.—Observational support for the white dwarf mass-radius relation, showing the positions of the visual binaries, common proper-motion systems, and field white dwarfs. The field white dwarf masses were derived using published surface gravity measurements and radii based on *Hipparcos* parallaxes.

4.1. *Tentative Suggestions of Iron-rich Cores*

Procyon B, EG 50, and GD 140 (labeled in Fig. 3) all lie significantly below the mass-radius relation for the expected carbon interior composition of white dwarfs. While the plot on the mass-radius relation may disguise the robust character of our result, a close look at Table 7 and Figures 3 and 4 shows the source of our suggestion that at least two of these three stars have iron-rich cores.

The masses predicted by the zero-temperature carbon-core mass-radius relation for GD 140 and EG 50, using the radii from Table 6, are considerable larger than the masses we observe, with 4 and 7 σ deviations (Fig. 3). GD 140 is a well-studied white dwarf (BSL) with ample spectroscopic evidence suggesting that it is massive. EG 50 is a more mysterious case. While at a similar temperature to GD 140, a comparison of the optical spectra presented in BSL shows that GD 140's Balmer lines are wider and shallower than EG 50's, arguing that GD 140 is more massive. Our radii from Table 6, combined with published values of log g, result in masses of $0.50 \pm 0.02\ M_\odot$ for EG 50, and $0.79 \pm 0.02\ M_\odot$ for GD 140, further supporting this comparison. BSL finds higher spectroscopic masses, assuming a carbon core and log He $= -4$ mass-radius relation, of 0.66 and $0.90 \pm 0.03\ M_\odot$ for EG 50 and GD 140, respectively. Our radii, combined with this same mass-radius relation, imply even higher masses of $\approx 0.8\ M_\odot$ (EG 50) and $\approx 0.95\ M_\odot$ (GD 140) (Fig. 4).

In essence, both EG 50 and GD 140 have radii that are significantly smaller than predicted by their observed masses, assuming the carbon-core mass-radius relation. The only way we can see of explaining the observations is by assume an iron, or an iron-rich, core composition. It is then possible to fit the observed radii, masses, and surface gravities consistently. It is conceivable that GD 140 harbors a core heavier than carbon. If, however, EG 50 is really a garden variety white dwarf with an average mass, we find it difficult to explain an iron core with current theories of white dwarf formation.

We discuss the problematic situation of Procyon B separately (Provencal et al. 1997). Even though our discussion does not incorporate the *Hipparcos* parallax, we

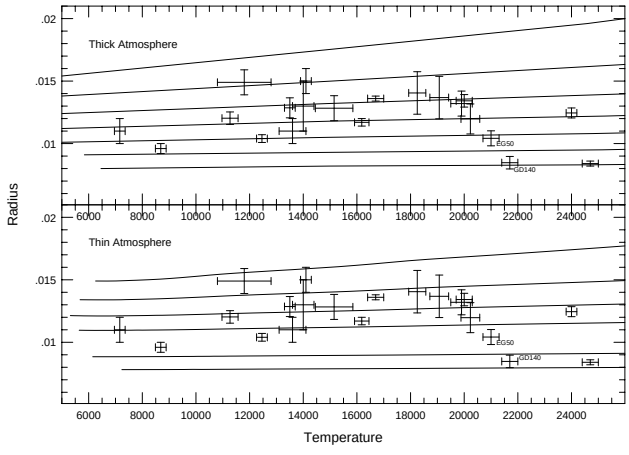

FIG. 4.—Predicted masses for our white dwarf sample based on the model used. The top panel uses models with thick [log q(H) $= -4$] surface layers, and the second has log q(H) $= 0$. The solid lines are white dwarf cooling curves at constant mass, beginning at $0.4\ M_\odot$ and increasing by 10ths sequentially downward. The error bars mark the 1 σ error positions for our observed points.

TABLE 7

COMPARISON OF WHITE DWARF MASSES

Object	$M_{\log}$ ($M_\odot$)	$M_{\rm spec}$ ($M_\odot$)	$M_{\rm gr}$ ($M_\odot$)	$M_{\rm astro}$ ($M_\odot$)
Binary Systems				
Procyon B				0.604 ± 0.018
Sirius B.....				1.000 ± 0.016
40 Eri B	0.47 ± 0.01	0.51 ± 0.03	0.50 ± 0.01	0.501 ± 0.011
CD−38 10980.....	0.71 ± 0.02	0.66 ± 0.02	0.74 ± 0.04	
G181-B5B.....	0.28 ± 0.10	0.47 ± 0.03	0.50 ± 0.03	
G154-B5B.....	0.31 ± 0.10	0.43 ± 0.03	0.46 ± 0.09	
G156-64	1.19 ± 0.18	0.86 ± 0.04	0.59 ± 0.06	
L268-92			0.70 ± 0.12	
Wolf 485 A	0.69 ± 0.02	0.54 ± 0.03	0.59 ± 0.04	
Field Stars				
GD279	0.44 ± 0.02	0.53 ± 0.03		
Feige 22	0.41 ± 0.03	0.48 ± 0.03		
EG 50	0.50 ± 0.02	0.66 ± 0.03		
EG 21	0.58 ± 0.05	0.63 ± 0.03		
GD 140	0.79 ± 0.02	0.90 ± 0.03		
G238-44	0.42 ± 0.01	0.55 ± 0.03		
G226-29	0.75 ± 0.03	0.70 ± 0.03		
WD2007-303.....	0.44 ± 0.05	0.51 ± 0.03		
Wolf 1346.....	0.44 ± 0.01	0.51 ± 0.03		
G93-48	0.75 ± 0.06	0.61 ± 0.03		
L711-10	0.54 ± 0.04	0.56 ± 0.03		

NOTE.—$M_{\rm spec}$ refers to spectroscopic masses from BSL and Bragaglia et al. 1995. $M_{\log}$ refers to masses derived using published surface gravities and radii calculated from *Hipparcos* parallaxes. $M_{\rm gr}$ is gravitational mass, and $M_{\rm astro}$ is the astrometric mass.

remain confronted with difficulties. We have no really solid information on Procyon B's photospheric composition, although WFPC2 photometry suggests helium. This limits our ability to fit model atmospheres to the data confidently. There is the additional complication that our data on Procyon B consist of magnitudes on the ST system, which have to be related to better understood ground-based systems.

4.2. *Thick Envelopes or Thin Envelopes*

Figures 2 and 3 illustrates a substantial spread in radius for stars with similar masses. For example, stellar radii around 0.6 $M_\odot$ range from 0.0096 (Procyon B) to 0.0150 (Wolf 485 A) $R_\odot$. To some extent, such a spread is expected, since there is a dependence of the mass-radius relation on the thickness of the models' hydrogen envelope. The question of thick versus thin atmosphere structure is discussed extensively in the literature (Shipman et al. 1997). BSL note that the masses of DA white dwarfs determined using models with thin or no hydrogen layers will be underestimated by approximately 0.04 $M_\odot$, if the actual atmospheres are thick.

Figure 4 presents the range of predicted masses based on our radii measurements, using the Wood (1995) mass-radius relations for thick and thin surface layer models. The top panel displays models with thick [log q(He) = −2, log q(H) = −4] surface layers, while the lower panel models have no hydrogen surface layers [log q(He) = −4, log q(H) = 0]. There is no appreciable radius difference between a model with log q(H) = −10 and one with log q(H) = 0. The solid lines are white dwarf cooling curves representing radii of models of various masses at different temperatures. The curves begin at 0.4 $M_\odot$ and increase by 10ths sequentially downward. A white dwarf of given mass would theoretically move from right to left along an appropriate track as it cools. The lower panel does not have a 0.8 $M_\odot$ track. The error bars mark the 1 σ error positions for all white dwarfs in our sample.

We concur with the results of BSL and find an average difference of 0.04 $M_\odot$ between the predictions of thick and thin models in Figure 4. Previous standard spectroscopic analysis leading from surface gravity to mass used models with thin or no hydrogen layers (BSL). Evidence is currently mounting, from spectroscopic (Barstow et al. 1993) and asteroseismological analysis (Clemens 1993), suggesting that most DA white dwarfs in fact have thick hydrogen layers of about log q(H) = −4.

While it is not yet possible to determine whether all white dwarfs have thick or thin atmospheres using the results of Figure 4, we believe it is possible to make such a determination for individual stars. For a particular star, we use Figure 4 and additional mass measurements from differing techniques to investigate whether the observed data are more consistent with thick or thin envelope models. Table 7 presents a comparison of mass measurements for various stars in our sample. The spectroscopic mass, $M_{\rm spec}$, is taken as published from either BSL or Bragaglia et al. (1995) and is derived from a mass-radius relation based on white dwarf models with no hydrogen surface layers. $M_{\log}$ is our recalculated spectroscopic mass using published surface gravities and the radii from Tables 3, 5, and 6. $M_{\log}$ does not rely on the mass-radius relation. $M_{\rm gr}$ is the gravitational redshift mass, and $M_{\rm astro}$ is the astrometric mass.

CD −38 10980 is a well-studied CPM white dwarf. Optical, UV, and EUV data indicate that this white dwarf has a relatively pure hydrogen atmosphere (Holberg et al. 1985; Vennes et al. 1996). BSL find $M_{\rm spec} = 0.66 \pm 0.02$ $M_\odot$, assuming log g = 8.10. Later work (Vennes et al. 1996;

Marsh et al. 1997) finds lower surface gravities of log $g = 7.98$ and 7.92, respectively. In any case, the spectroscopic mass is significantly lower than M_{gr}. These results are consistent with the arguments of BSL, assuming CD -38 10980 actually has a thick hydrogen surface layer. Figure 4 further supports this conclusion. The thick surface layer model predicts a mass of 0.69 $M_\odot$, a better fit to the gravitational mass than the 0.63 $M_\odot$ predicted by a thin model. Based on these results, we suggest that CD -38 10980 has a thick hydrogen surface layer. A similar case can be argued for Wolf 485 A, where M_{spec} is again significantly lower than either M_{gr} or M_{log}.

On the other hand, Shipman et al. (1997) perform a similar analysis of 40 Eri B. Table 7 shows that 40 Eri B's M_{gr}, M_{log}, and M_{astro} are in good agreement with M_{spec}. Thick–hydrogen atmosphere models predict a mass of $\approx 0.59\ M_\odot$, well above both the gravitational and astrometric determinations for this star. Therefore, we are reasonably confident that 40 Eri B has a thin hydrogen atmosphere. Combined with CD -38 10980 and Wolf 485 A, these findings support other investigations (Shipman 1984) arguing that the ratio of DAs to non-DAs at cooler temperatures indicates that DAs do not have the same envelope structure but span a range of hydrogen layer thicknesses from 10^{-4} to $10^{-7}\ M_\odot$.

4.3. *Photospheric Helium*

A second possible consideration is the undetected presence of helium. BSL convincingly demonstrates that at temperatures below 12,000 K, large amounts of spectroscopically invisible helium brought to the surface by convection can produce pressure effects that are indistinguishable from increased surface gravity. In essence, cool DA white dwarfs with large surface gravities can be interpreted as helium-rich stars with normal masses. A substantial fraction of visual binaries and CPM systems included in our study, G181-B5B, G154-B5B, G156-64, Wolf 485 A, L268-92, Procyon B, and Stein 2051 B have temperatures below 15,000 K, where convection is important. All of the field stars, with the exception of G226-29, are above 15,000 K.

The key to distinguishing helium's presence may come from a comparison of gravitational and spectroscopic masses. The non-LTE core of Hα commonly used in gravitational velocity measurements is least affected by pressure shifts of all the hydrogen lines. For four of the five CPM systems below 15,000 K, M_{log} does differ significantly from M_{gr}. G156-64, the coolest white dwarf in our sample at 7200 ± 200 K, offers the best case for the presence of helium. Its gravitational mass ($0.59 \pm 0.06\ M_\odot$) is consistent with that of a garden variety white dwarf. However, M_{log} argues that this white dwarf is more massive than Sirius B. While it would be nice to have another massive white dwarf to help pin down the high-mass end of the mass-radius relation, this result instead suggests that an additional source of pressure, probably helium, is mimicking increased surface gravity.

It is clear, however, that helium does not play a strong role either in G181-B5B or in G154-B5B. For these two objects, M_{log} is lower than M_{gr}.

4.4. *The ZZ Ceti Instability Strip and Convection*

Finally, we point out that our white dwarf sample includes one ZZ Ceti star, G226-29. G226-29 is the brightest and closest known DA nonradial pulsator. G226-29 has been the subject of intense photometric investigation by the Whole Earth Telescope (Kepler et al. 1995), two results of which are a mass estimate near 0.8 $M_\odot$ and a thick hydrogen surface layer (log $M_H = -4$; Bradley 1995). However, controversy persists regarding its effective temperature, either at 13,600 or at 12,100 K. This controversy has important implications not solely for G226-29, but also for the location of the ZZ Ceti instability strip, in turn influencing our understanding of convective efficiency in these stars. Bergeron et al. (1995c) present a convincing analysis determining a temperature of 12,400 K for G226-29. The authors then place the instability strip at $12{,}460 \geq T_{eff} \geq 11{,}160$ K and deduce a convective efficiency between that of ML2 and ML1, using the mixing length theory nomenclature first introduced by Fontaine, Villeneuve, & Wilson (1981). In brief, ML2 has a convective efficiency greater than ML1. The *Hipparcos* parallax for G226-29 supports these conclusions. Combining an effective temperature of 12,460 K and log $g = 8.29$ as determined by Bergeron et al. (1995c) for a convective efficiency of ML2/$\alpha = 0.6$, between that of ML1 and ML2, we find a radius of $0.0104 \pm 0.0003\ R_\odot$. Assuming a thick–hydrogen atmosphere mass-radius relation, we find a stellar mass of $0.77 \pm 0.04\ M_\odot$, in agreement with the asteroseismological results. A temperature of 13650 K and its corresponding log $g = 8.14$ for more efficient ML2 models (Bergeron et al. 1995c) results in a stellar mass of $0.47 \pm 0.04\ M_\odot$, which is in strong disagreement with the asteroseismological mass. Therefore, our results support both the lower temperature and a convective efficiency between ML1 and ML2.

5. CONCLUSIONS

Hipparcos parallaxes give us vital distance information that enables us to improve the empirical underpinnings of the white dwarf mass-radius relation. Visual binaries and CPM systems remain the backbone of observational support. Unfortunately, the prospects for significant improvement in our knowledge of white dwarf masses and radii does not look terribly bright in the short term. An examination of Tables 3 and 5 suggests that parallax remains a dominant source of uncertainty, especially for the CPM systems. While waiting for the next generation of satellites and ground-based observations to provide ever more precise parallaxes, we can gain some improvement in the precision of observed masses and radii of both the visual binaries and the CPM systems by improving ground-based determinations of orbital parameters, effective temperatures, gravitational velocities, and, surprisingly, magnitudes. We can also expect to add three new points to Figures 2 and 3, through improved observations of the binary V471 Tau and determinations of the parameters of the white dwarf binary G107-70AB. The precision of these new points remains to be seen.

Unlike visual binaries or CPM systems, mass determinations for field white dwarfs are indirect, relying solely on the comparison of observed spectra with detailed, complicated model-atmosphere predictions. Many studies, for example, BSL, Bragaglia et al. (1995), and Bergeron et al. (1995c), demonstrate that such results are model dependent and may be further complicated by additional, unconsidered sources of pressure. Our goals should include not only improving the atmosphere models themselves, but also understanding the differences behind the model depen-

dence, improving our treatment of convection, and reducing observational errors. Asteroseismological masses from the ZZ Ceti pulsators will be of great value. Unfortunately, the DA pulsators have proven difficult subjects for asteroseismology, because they exhibit too few excited modes (Kepler et al. 1995).

Hipparcos parallaxes not only enable us to improve the observational support of the white dwarf mass-radius relation, but they also allow us to develop tools to investigate related fields, such as white dwarf structure. Our results present evidence that all DA white dwarfs do not have the same hydrogen surface layer thickness. Although we don't have sufficient information to provide a detailed atmospheric thickness distribution, the existence of such a range must be taken into account by theories of white dwarf formation and evolution.

We live in interesting times; future work will be exciting. We are poised on the verge not only of probing white dwarf atmospheric structure but also of differentiating between white dwarfs of various core compositions. While most white dwarfs are assumed to harbor carbon or carbon/oxygen cores, we have no observational evidence for such an assumption. Three objects in our study, GD 140, EG 50, and Procyon B have radii that are much smaller than predicted by their observed masses. One interpretation of this result is the presence of an iron core. The mysterious Procyon B offers perhaps the best possibility for a precise investigation of the mass-radius relation. We estimate that a reduction in errors in effective temperature from ± 200 to ± 60 K will reduce the radius errors by $\approx 75\%$, which is the precision we require for determining if this star really has an iron core. This accuracy, considering the high quality of Space Telescope Imaging Spectrograph spectra, is within our reach.

This work is based on data from the ESA *Hipparcos* astrometry satellite. This work is supported in part by NASA grants NAGW-4812 and NAG 5-2405, and GO-2593.0187A and GO-3816.01. H. L. S. also acknowledges the long-term support of the NSF, and P. T. acknowledges support from Nordita. J. L. P. would like to thank D. Huber and P. Bradley for helpful discussions. This research made use of the Simbad database, operated at CDS, Strasbourg, France.

REFERENCES

Barstow, M. A., et al. 1993, MNRAS, 264, 16
Bergeron, P., Liebert, J., & Fulbright, M. S. 1995a, ApJ, 444, 810
Bergeron, P., Saffer, R. A., & Liebert, J. 1992, ApJ, 394, 228 (BSL)
Bergeron, P., Wesemael, F., & Beauchamp, A. 1995b, PASP, 107, 1047
Bergeron, P., Wesemael, F., Lamontagne, R., Fontaine, G., Saffer, R. A., & Allard, N. F. 1995c, ApJ, 449, 258
Bois, B., Mochnacki, S. W., & Lanning, H. H. 1988, AJ, 96, 157
Borgman, E. R., & Lippincott, S. L. 1983, AJ, 88, 120
Bradley, P. A. 1995, in IAU Colloq. 155, Astrophysical Applications of Stellar Pulsation, ed. R. S. Stobie & P. A. Whitelock (San Francisco: ASP), 251
Bragaglia, A., Renzine, A., & Bergeron, P. 1995, ApJ, 443, 735
Chandrasekhar, S. 1933, MNRAS, 93, 390
Clemens, J. C. 1993, Ph.D. thesis, University of Texas
European Space Agency. 1997, The *Hipparcos* and Tycho Catalogues (Noordwijk, Netherlands: ESA SP-1200)
Fontaine, G., Villeneuve, B., & Wilson, J. 1981, ApJ, 243, 550
Gatewood, G. D., & Gatewood, C. V. 1978, ApJ, 225, 191
Girard, T. M., Wu, H., Lee, J. T., Dyson, S. E., Horch, E. P., Van Altena, W. F., & Ftaclas, C. 1996, BAAS, 188, 6002
Grabowski, B., Madej, J., & Halenka, J. 1987, ApJ, 313, 683
Hamada T., & Salpeter, E. E. 1961, ApJ, 134, 683
Harrington, R. S., et al. 1993, AJ, 105, 1571
Heintz, W. D. 1974, AJ, 79, 819
Holberg, J. B., Bruhweiler, F. C., & Andersen, J. 1995, ApJ, 443, 753
Holberg, J. B., Wesemael, F., Wegner, G., & Bruhweiler, F. C. 1985, ApJ, 293, 294
Kepler, S. O., et al. 1995, ApJ, 447, 874
Kidder, K. M. 1991, Ph.D. thesis, University of Arizona
Kidder, K. M., Holberg, J. B., & Mason, P. A. 1991, AJ, 101, 579
Koester, D. 1987, ApJ, 322, 852
Koester, D., & Weidemann, V. 1991, AJ, 102, 1152
Kovalevsky, J., et al. 1992, A& A, 258, 7
Landolt, A. U. 1992, AJ, 104, 372
Liebert, J. 1976, ApJ, 210, 715
Lindegren, L., et al. 1992, A&A, 258, 18
Marsh, M. C., et al. 1997, MNRAS, 286, 369
Perryman, M. A. C., et al. 1992, A&A, 258, 1
Provencal, J. L., Shipman, H. L., Wesemael, F., Bergeron, P., Bond, H. E., Liebert, J., & Sion, E. M. 1997, ApJ, 480, 777
Reid, I. N. 1996, AJ, 111, 2000
Schmidt, H. 1996, A&A, 311, 852
Shipman, H. L. 1979, ApJ, 228, 240
———. 1984, in IAU Colloq. 114, White Dwarfs, ed. G. Wegner (New York: Springer), 220
Shipman, H. L., Provencal, J. L., Hϕg, E., & Thejll, P. 1997, ApJ, 488, L43
Shipman, H. L., & Sass, C. A. 1980, ApJ, 235, 177
Strand, K. Aa. 1977, AJ, 82, 745
van Altena, W. F., Lee, J. T., & Hoffleit, D. E. 1995, The General Catalogue of Trigonometric Parallaxes (4th ed.; Yale Univ. Observatory)
Vauclair, G., Schmidt, H., Koester, D., & Allard, N. 1997, A&A, submitted
Vennes, S., Thejll, P., Wickramasinghe, D. T., & Bessell, M. S. 1996, ApJ, 467, 782
Wegner, G., & Reid, I. N. 1987, in IAU Colloq. 95, Second Conference on Faint Blue Stars, ed. A. G. D. Philip, D. S. Hayes, & J. W. Liebert (Schenectady: L. Davis), 649
———. 1991, ApJ, 375, 674
Wood, M. A. 1990, Ph.D. thesis, University of Texas at Austin
———. 1995, in Proc. 9th European Workshop on White Dwarfs, ed. D. Koester & K. Werner (Berlin: Springer), 41